Int. J. Heat Mass Transfer. Vol. 26, No. 2, pp. 231–243, 1983
Printed in Great Britain

0017-9310/83/020231-13 $03.00/0

NATURAL CONVECTION FROM HORIZONTAL CYLINDERS IN INTERACTING FLOW FIELDS

B. FAROUK
Department of Mechanical Engineering and Mechanics, Drexel University, Philadelphia, PA 19104, U.S.A.

and

S. İ. GÜÇERI
Department of Mechanical and Aerospace Engineering, University of Delaware, Newark, DE 19711, U.S.A.

(*Received* 11 *January* 1982 *and in final form* 10 *June* 1982)

Abstract—Natural convection heat transfer from single and double rows of closely spaced isothermal heated cylinders was investigated numerically for both laminar and turbulent cases. A sufficiently large number of cylinders are considered in each row such that a symmetry unit can be considered for the analysis. The numerical scheme involves the use of a cylindrical network of nodes in the vicinity of the cylinder with a Cartesian mesh covering the remainder of the flow domain. The k–ε turbulence model has been applied to obtain the results for the turbulent flow predictions. Effects of varying the cylinder spacings in the horizontal direction are also considered. The results are of direct use in electrical packaging, solar heating and storing technology, nuclear reactor safety and waste disposal, among others.

NOMENCLATURE

C_μ, C_1, C_2, C_3, empirical turbulence model constants;
c_p, specific heat at constant pressure;
D, cylinder diameter;
g, gravitational acceleration;
Gr, Grashof number, $\rho^2 g\beta D^3 (T_w - T_\infty)/\mu^2$;
k, turbulent kinetic energy, $(1/2)\overline{(v_r'^2 + v_\theta'^2 + v_z'^2)}$ or $(1/2)\overline{(v_x'^2 + v_y'^2 + v_z'^2)}$;
k^*, dimensionless turbulent kinetic energy, D^2k/ν^2;
l, characteristic length scale of turbulence;
Pr, Prandtl number, $\mu c_p/\lambda$;
r, radial coordinate;
r^*, dimensionless radial coordinate, r/D;
Ra, Rayleigh number, $Gr\,Pr$;
S_L, horizontal center-to-center distance for an array of cylinders;
S_T, vertical center-to-center distance for an array of cylinders;
T, local temperature;
T_w, cylinder surface temperature;
T_∞, ambient temperature;
T^*, dimensionless temperature, $(T - T_\infty)/(T_w - T_\infty)$;
v_r, radial velocity component;
v_r^*, dimensionless radial velocity component, $\rho D v_r/\mu$;
v_θ, circumferential velocity component;
v_θ^*, dimensionless circumferential velocity component, $\rho D v_\theta/\mu$;
v_x, velocity component in the x direction;
v_x^*, dimensionless velocity component in the x direction, $\rho D v_x/\mu$;
v_y, velocity component in the y direction;
v_y^*, dimensionless velocity component in the y direction, $\rho D v_y/\mu$;
x, Cartesian coordinate denoting horizontal distance;
x^*, dimensionless x coordinate, x/D;
y, Cartesian coordinate denoting vertical distance;
y^*, dimensionless y coordinate, y/D;
z, axial coordinate.

Greek symbols

β, thermal coefficient of volume expansion;
ε, volumetric dissipation rate of turbulent kinetic energy;
ε^*, dimensionless volumetric dissipation rate of turbulent kinetic energy, $D^4\varepsilon/\nu^3$;
θ, circumferential (angle) coordinate;
λ, thermal conductivity;
μ, molecular viscosity;
μ_t, turbulent viscosity;
μ_t^*, dimensionless turbulent viscosity, μ_t/μ;
ρ, density;
ν, kinematic viscosity;
ψ, stream function;
ψ^*, dimensionless stream function, ψ/μ;
ω, vorticity component parallel to cylinder axis;
ω^*, dimensionless vorticity, $D^2\omega/\nu$.

INTRODUCTION

THE STUDY of forced convection heat transfer in interacting flow fields (e.g. flows normal to a bank of tubes) received considerable attention in the past because of the importance of the flow configuration in the design of heat exchangers [1–5]. Investigations in

the area of heat transfer by natural convection from tube banks or arrays of cylinders, where separate flow fields induced by individual surfaces interact, have been, up to now, relatively few. The mathematical complexities are much more involved than the forced convection case. The interest in obtaining quantitative information about natural convection heat transfer in interacting flow fields has increased considerably in the last decade. This has been mainly due to advances in electrical packaging, solar heating technology, nuclear reactor safety and the handling of nuclear wastes. The demands for energy conservation have also increased the importance for a better understanding of natural convection in interacting flow-fields.

Eckert and Soehngen [6] used a Zehnder–Mach interferometer to study natural convection from a cluster of heated horizontal cylinders placed in an infinite medium. It was observed that the effect of the warmer wake around the upper cylinders reduced the heat transferred since the temperature differential had decreased. For a staggered arrangement of the cylinders, an induced fluid movement of cooler air resulted in a greater heat transfer. Leiberman and Gebhart [7] experimentally investigated the interaction between the natural convective flows of several closely spaced surfaces by using long, horizontal wires in a parallel array at several spacings and inclinations. The influence of tube spacing and array on natural convection heat transfer for horizontal tube bundles has been determined experimentally by Tillman [8]. Tillman concluded that tube spacing has more effect on the heat transfer than the type of array. Natural convection from vertical tube bundles to an infinite atmosphere has been studied experimentally by Davis and Perona [9].

Recently, Warrington and Crupper [10] have experimentally investigated natural convection heat transfer from a fixed array of four isothermal cylinders in a cubical enclosure. The cylinders were placed both vertically and horizontally and it was observed that the vertical configuration led to decreased heat transfer.

The purpose of this study is to obtain solutions to the complete Navier–Stokes and energy equations for steady state 2-dim. laminar and turbulent natural convection in interacting flow-fields. This refers to a flow field where the buoyancy-driven flow is caused by more than one heated body. Specifically, rows of isothermal horizontal cylinders are considered submerged in an infinite Boussinesq fluid. Previous numerical studies of forced convection in tube banks [4, 5] considered fully developed flows where a "representative element" of the cross-section is considered remote from the influence of the boundaries. The governing equations are solved for this element by considering repetitive boundary conditions at the inlet and outlet regions. Unfortunately, such an approach is not applicable to *natural convection* in a tube bank because of the strong coupling between the momentum and energy equations and the unknown mass flow rate through the tube bank. Whereas for forced convection analysis the mass flow rate is independent of number of tubes in the bank and their spacings, it is not the case for natural convection.

SINGLE AND DOUBLE ROWS OF CYLINDERS

To study the interactions between the natural convective flows of closely spaced bodies, single and double rows of circular cylinders placed equally apart are considered. A finite difference numerical scheme [11], which has recently been applied to natural convection problems [12–14], is adopted for generating the 2-dim. steady state results. A symmetry unit is considered for both the single and double rows of cylinders as shown in Figs. 1–3. The ratio (S_L/D) of the center-to-center distance between the cylinders in the horizontal direction to the cylinder diameter was varied from 6 to 2 for the case of a single row of cylinders. For double rows of cylinders the spacings between the cylinders in the vertical (S_T) and horizontal directions (S_L) were kept equal to 4 for the results presented.

A two equation (k–ε) turbulence model was used to predict the natural convective flow in the interactive flow-field for Rayleigh numbers above 10^7. The flow around a single heated cylinder tends to become turbulent when the Rayleigh number exceeds the above value [16]. The k-ε model proposed by Launder and Spalding [15], characterizes turbulence by transport equations for time averaged k, the turbulent

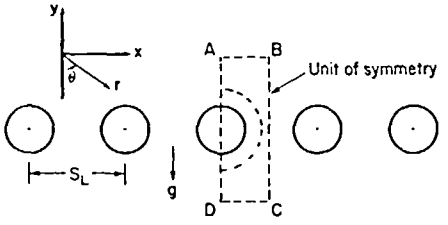

FIG. 1. Single row of cylinders with the unit of symmetry indicated.

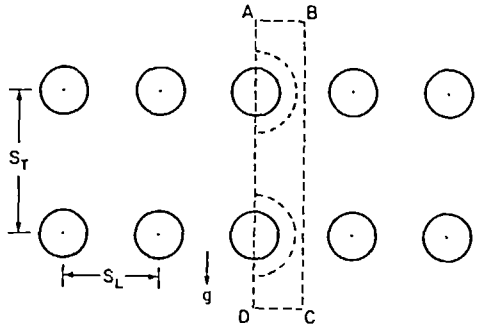

FIG. 2. Double rows of in-line cylinders with the unit of symmetry indicated.

kinetic energy and ε, its rate of dissipation. Buoyancy effects on the turbulence structure are also accounted for. The equations for the time averaged continuity, momentum and energy are solved simultaneously with the differential equations for k and ε for the turbulent flow predictions. In order to limit the size of the flow domain, an S_L/D ratio of 2 is used only for generating results in the turbulent regime. Turbulent flow predictions were obtained for the "single row" case only.

Air properties at atmospheric pressure were used in the following calculations with $Pr = 0.721$. The applicability of the method used is, however, not limited to the above geometrical configurations and the Prandtl number studied.

THE FINITE DIFFERENCE GRID SYSTEM

For the finite difference solution of elliptic equations, the flow boundaries should be grid lines themselves, otherwise either an uneven boundary will result or special finite difference formulae will be needed at the boundary. This constraint is more important at a solid boundary since any mismatch here between the grid and the boundary could lead to an erroneous flow pattern. Considering the symmetry units depicted in Figs. 1–3, it is seen that the main deterrent is the circular boundary of the cylinders as opposed to the rectangular boundary of the flow domain.

A composite form of polar and Cartesian system of grids, recently suggested by Launder and Massey [5], has been employed in this study. Close to the cylinder, the steepest gradients of flow properties are in the radial directions. Thus, a cylindrical polar grid in the neighbourhood of the cylinder was retained. The r coordinate is measured from the center of the cylinders and θ is measured anti-clockwise from the downward vertical line as shown in Fig. 1. The remaining flow region is filled with a Cartesian mesh. For the double rows case, two polar grid systems are used in the vicinity of two cylinders within the symmetry unit. The cylindrical and Cartesian grids are entirely independent of one another. However, the grids overlap each other and no matching of nodes between neighboring grid regions was attempted. A line of "false" nodes was defined, for each grid, beyond the intersection line to provide a connection between the cylindrical and polar regions. Additional details of the matching region can be found elsewhere [5, 17]. This system of the composite grid was chosen for the present problem as it is found to be flexible and capable of modelling any pitch-to-diameter ratio for the rows of cylinders considered.

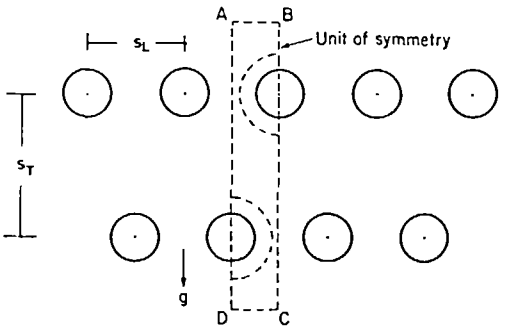

FIG. 3. Double rows of staggered cylinders with the unit of symmetry indicated.

MATHEMATICAL FORMULATION

Using the stream function–vorticity approach, the steady state 2-dim. laminar natural convection in the interacting flow-field considered is given by the coupled elliptic transport equations for ψ^*, ω^*, and T^*.

Various authors have proposed closure models for turbulent flows in an attempt to accurately predict the turbulent shear stress. Due to its demonstrated success in calculating a wide variety of forced flows, the k–ε model of Launder and Spalding [15] was chosen for calculating the turbulent natural convection in the interacting flow-fields. The turbulent viscosity is proportional to a characteristic velocity of turbulence (e.g. the square root of the turbulent kinetic energy) and a length scale representing the energy-containing eddies. In the k–ε model under consideration the length scale is taken to be the dissipation length scale ($\varepsilon \sim k^{3/2}/l$). Thus, the turbulent viscosity can be written as

$$\mu_t = C_\mu \rho k^2/\varepsilon \tag{1}$$

where C_μ is an empirical constant. In the turbulence model employed, time averaged values of the temperature $\bar{T}^*$, stream function $\bar{\psi}^*$ and vorticity $\bar{\omega}^*$ are used. The mean motion is considered to be 2-dim., but fluctuating components of velocities in all three dimensions are taken into account. The partial differential equations for steady (time averaged) turbulent natural convection flow can be written in cylindrical polar coordinate form using the Boussinesq approximation as follows:

$$\frac{\partial}{\partial r^*}\left(r^* \frac{\partial \bar{\psi}^*}{\partial r^*}\right) + \frac{\partial}{\partial \theta}\left(\frac{1}{r^*}\frac{\partial \bar{\psi}^*}{\partial \theta}\right) = -r^* \bar{\omega}^*, \tag{2}$$

$$\frac{\partial}{\partial r^*}\left(\bar{\omega}^* \frac{\partial \bar{\psi}^*}{\partial \theta^*}\right) - \frac{\partial}{\partial \theta}\left(\omega^* \frac{\partial \bar{\psi}^*}{\partial r^*}\right) - \frac{\partial}{\partial r^*}\left\{r^* \frac{\partial[(1+\mu_t^*)\bar{\omega}^*]}{\partial r^*}\right\} - \frac{\partial}{\partial \theta}\left\{\frac{1}{r^*}\frac{\partial[(1+\mu_t^*)\omega^*]}{\partial \theta}\right\} = Gr\left(\frac{\partial \bar{T}^*}{\partial \theta}\cos\theta + \frac{\partial \bar{T}^*}{\partial r^*} r^* \sin\theta\right), \tag{3}$$

$$\frac{\partial}{\partial r^*}\left(\bar{T}^* \frac{\partial \bar{\psi}^*}{\partial \theta}\right) - \frac{\partial}{\partial \theta}\left(\bar{T}^* \frac{\partial \bar{\psi}^*}{\partial r^*}\right) - \frac{\partial}{\partial r^*}\left\{\left(\frac{1}{Pr} + \frac{\mu_t^*}{\sigma_T}\right) r^* \frac{\partial \bar{T}^*}{\partial r^*}\right\} - \frac{\partial}{\partial \theta}\left\{\left[\frac{1}{Pr} + \frac{\mu_t^*}{\sigma_T}\right]\frac{1}{r^*}\frac{\partial \bar{T}}{\partial \theta}\right\} = 0, \tag{4}$$

$$\frac{\partial}{\partial r^*}\left(k^*\frac{\partial \bar{\psi}^*}{\partial \theta}\right)-\frac{\partial}{\partial \theta}\left(k^*\frac{\partial \bar{\psi}^*}{\partial r^*}\right)$$
$$-\frac{\partial}{\partial r^*}\left[\left(1+\frac{\mu_t^*}{\sigma_k}\right)r^*\frac{\partial k^*}{\partial r^*}\right]$$
$$-\frac{\partial}{\partial \theta}\left[\left(1+\frac{\mu_t^*}{\sigma_k}\right)\frac{1}{r^*}\frac{\partial k^*}{\partial \theta}\right]=-r^*S_k \quad (5a)$$

where

$$S_k=-\mu_t^*\left\{2\left(\frac{\partial \bar{v}_r^*}{\partial r^*}\right)^2+2\left(\frac{\partial \bar{v}_\theta^*}{r^*\partial\theta}\right)^2+2\left(\frac{\bar{v}_r^*}{r^*}\right)^2+\left[r^*\frac{\partial}{\partial r^*}\left(\frac{\bar{v}_\theta^*}{r^*}\right)+\frac{\partial \bar{v}_r^*}{r^*\partial\theta}\right]^2\right\}+Gr\frac{\mu_t^*}{\sigma_T}\left(\frac{\partial \bar{T}}{r^*\partial\theta}\sin\theta-\frac{\partial \bar{T}^*}{\partial r^*}\cos\theta\right)+\varepsilon^* \quad (5b)$$

and

$$\frac{\partial}{\partial r^*}\left(\varepsilon^*\frac{\partial \bar{\psi}^*}{\partial\theta}\right)-\frac{\partial}{\partial\theta}\left(\varepsilon^*\frac{\partial \bar{\psi}^*}{\partial r^*}\right)$$
$$-\frac{\partial}{\partial r^*}\left[\left(1+\frac{\mu_t^*}{\sigma_\varepsilon}\right)r^*\frac{\partial \varepsilon^*}{\partial r^*}\right]$$
$$-\frac{\partial}{\partial\theta}\left[\left(1+\frac{\mu_t^*}{\sigma_\varepsilon}\right)\frac{1}{r^*}\frac{\partial \varepsilon^*}{\partial\theta}\right]=-r^*S_\varepsilon \quad (6a)$$

where

$$S_\varepsilon=-C_1\mu_t^*\frac{\varepsilon^*}{k^*}\left\{2\left(\frac{\partial \bar{v}_r^*}{\partial r^*}\right)^2+2\left(\frac{\partial \bar{v}_\theta^*}{r^*\partial\theta}\right)^2+2\left(\frac{\bar{v}_r^*}{r^*}\right)^2+\left[r^*\frac{\partial}{\partial r^*}\left(\frac{\bar{v}_\theta^*}{r^*}\right)+\frac{\partial \bar{v}_r^*}{r^*\partial\theta}\right]^2\right\}+C_3Gr\frac{\mu_t^*}{\sigma_T}\frac{\varepsilon^*}{k^*}\left(\frac{1}{r^*}\frac{\partial \bar{T}^*}{\partial\theta}\sin\theta-\frac{\partial \bar{T}^*}{\partial r^*}\cos\theta\right)+C_2\frac{\varepsilon^{*2}}{k^*} \quad (6b)$$

and the stream function and the vorticity are defined as

$$\bar{v}_r^*=\frac{1}{r^*}\frac{\partial \bar{\psi}^*}{\partial\theta};\quad \bar{v}_\theta^*=-\frac{\partial \bar{\psi}}{\partial r^*}, \quad (7a, 7b)$$

$$\bar{\omega}^*=\frac{1}{r^*}\left[\frac{\partial}{\partial r^*}(r^*\bar{v}_\theta^*)-\frac{\partial \bar{v}_r^*}{\partial\theta}\right]. \quad (8)$$

The above equations are used in the vicinity of the cylinder. This set of equations in the Cartesian coordinates become

$$\frac{\partial}{\partial x^*}\left(\frac{\partial \bar{\psi}^*}{\partial x^*}\right)+\frac{\partial}{\partial y^*}\left(\frac{\partial \bar{\psi}^*}{\partial y^*}\right)=-\bar{\omega}^*, \quad (9)$$

$$\frac{\partial}{\partial x^*}\left(\bar{\omega}^*\frac{\partial \bar{\psi}^*}{\partial y^*}\right)-\frac{\partial}{\partial y^*}\left(\bar{\omega}^*\frac{\partial \bar{\psi}^*}{\partial x^*}\right)$$
$$-\frac{\partial}{\partial x^*}\left\{\hat{c}[(1+\mu_t^*)\bar{\omega}^*]\right\}$$
$$-\frac{\partial}{\partial y^*}\left\{\hat{c}[(1+\mu_t^*)\bar{\omega}^*]\right\}=Gr\frac{\partial \bar{T}^*}{\partial x^*}, \quad (10)$$

$$\frac{\partial}{\partial x^*}\left(\bar{T}^*\frac{\partial \bar{\psi}^*}{\partial y}\right)-\frac{\partial}{\partial y^*}\left(\bar{T}^*\frac{\partial \bar{\psi}^*}{\partial x^*}\right)$$
$$-\frac{\partial}{\partial x^*}\left[\left(\frac{1}{Pr}+\frac{\mu_t^*}{\sigma_T}\right)\frac{\partial \bar{T}^*}{\partial x^*}\right]$$
$$-\frac{\partial}{\partial y^*}\left[\left(\frac{1}{Pr}+\frac{\mu_t^*}{\sigma_T}\right)\frac{\partial \bar{T}^*}{\partial y^*}\right]=0, \quad (11)$$

$$\frac{\partial}{\partial x^*}\left(k^*\frac{\partial \bar{\psi}^*}{\partial y^*}\right)-\frac{\partial}{\partial y^*}\left(k^*\frac{\partial \bar{\psi}^*}{\partial x^*}\right)-\frac{\partial}{\partial x^*}\left[\left(1+\frac{\mu_t^*}{\sigma_k}\right)\times\frac{\partial k^*}{\partial x}\right]-\frac{\partial}{\partial y^*}\left[\left(1+\frac{\mu_t^*}{\sigma_k}\right)\frac{\partial k^*}{\partial y^*}\right]=-S_k' \quad (12a)$$

where

$$S_k'=-\mu_t^*\left[2\left(\frac{\partial \bar{v}_x^*}{\partial x}\right)^2+2\left(\frac{\partial \bar{v}_y^*}{\partial y^*}\right)^2+\left(\frac{\partial \bar{v}_x^*}{\partial y^*}+\frac{\partial \bar{v}_y^*}{\partial x^*}\right)^2\right]+Gr\frac{\mu_t^*}{\sigma_T}\left(\frac{\partial \bar{T}^*}{\partial y}\right)+\varepsilon^* \quad (12b)$$

and

$$\frac{\partial}{\partial x^*}\left(\varepsilon^*\frac{\partial \bar{\psi}^*}{\partial y^*}\right)-\frac{\partial}{\partial y^*}\left(\varepsilon^*\frac{\partial \bar{\psi}^*}{\partial x^*}\right)-\frac{\partial}{\partial x^*}\left[\left(1+\frac{\mu_t^*}{\sigma_\varepsilon}\right)\frac{\partial \varepsilon^*}{\partial x^*}\right]-\frac{\partial}{\partial y^*}\left[\left(1+\frac{\mu_t^*}{\sigma_\varepsilon}\right)\frac{\partial \varepsilon^*}{\partial y^*}\right]=-S_\varepsilon' \quad (13a)$$

where

$$S_\varepsilon'=-C_1\mu_t\frac{\varepsilon^*}{k^*}\left[2\left(\frac{\partial \bar{v}_x^*}{\partial x}\right)^2+2\left(\frac{\partial \bar{v}_y^*}{\partial y^*}\right)^2+\left(\frac{\partial \bar{v}_x^*}{\partial y^*}+\frac{\partial \bar{v}_y^*}{\partial x^*}\right)^2\right]+C_3Gr\frac{\mu_t^*}{\sigma_T}\frac{\varepsilon^*}{k^*}\left(\frac{\partial \bar{T}^*}{\partial y^*}\right)+C_2\frac{\varepsilon^{*2}}{k^*} \quad (13b)$$

where the stream function and the vorticity are defined as

$$\bar{v}_x^*=\frac{\partial \bar{\psi}^*}{\partial y^*};\quad \bar{v}_y^*=-\frac{\partial \bar{\psi}^*}{\partial x^*} \quad (14a, 14b)$$

and

$$\bar{\omega}^*=\frac{\partial \bar{v}_y^*}{\partial x^*}-\frac{\partial \bar{v}_x^*}{\partial y^*}. \quad (15)$$

For forced convection flows, turbulence energy is created by the action of the turbulent contribution to the shear stresses on the moving fluid. In natural convection flows, however, a buoyancy induced source of turbulent kinetic energy is also present. The expressions (5b) and (12b) represent the energy production and/or dissipation terms for the k^* equation in polar and Cartesian coordinates, respectively.

This model contains empirical constants in the preceding expressions. σ_T, σ_k, and σ_ε are the turbulent Prandtl numbers for $\bar{T}^*$, k^*, and ε^* respectively. Numerical values for C_μ, C_1, C_2, σ_T, σ_k, and σ_ε are taken as recommended by Spalding and Launder [15].

The constant C_3 does not exist in forced flows, but its value can be chosen to be equal to C_1 implying similar contribution from buoyant and gradient production on the scales and intensity of the turbulence. Previous studies [13, 14, 18] have shown that variation of C_3 has slight effect on the heat transfer predictions. The numerical values for the empirical constants used in this study are given in Table 1.

It should be noted that both the molecular viscosity and the laminar Prandtl number have been taken into account in the turbulent form of the equations. Thus, the equations are valid throughout the laminar, semi-laminar and turbulent regions of the flow field [15].

For laminar flow predictions, only equations for ψ^*, ω^*, and T^* are considered and these are obtained by setting $\mu_t^* = 0$ and dropping the over-bars in equations (2)–(4) for cylindrical coordinates and equations (9)–(11) for Cartesian coordinates.

BOUNDARY CONDITIONS

The coupled set of elliptic equations (three for the laminar case and five for the turbulent case) can only be solved if the conditions are specified along the entire boundary which encloses the flow field. The cylinders are considered to be held at a uniform temperature T_w ($T_w > T_\infty$). The necessity to limit the size of the solution domain requires that inflow and outflow boundaries be defined at finite distances upstream and downstream from the cylinders.

The boundary sections considered in the solution domain A–B–C–D (as shown in Figs. 1–3) are handled as follows:

Symmetry lines

On the left symmetry line A–D, the stream function is set equal to zero. Vorticity and the gradient of the temperature normal to the symmetry lines A–D and B–C are both set to zero. For the case of turbulent flow predictions, the gradients of k^* and ε^* normal to the symmetry lines are also set to zero.

A major difficulty in the solution of the set of equations considered is the mass flow rate which is not known *a priori*, both in terms of magnitude and distribution. Along the symmetry line B–C, the value of the stream function is uniform, considering no flow across it. An iterative scheme was used to evaluate the stream function. For every iteration cycle, the stream function value along the symmetry line B–C is set equal to the average of the stream function values at the nodes nearest to the symmetry line at the inflow and outflow sections, calculated from the previous iteration cycle. This way of handling the stream function boundary condition provided converged solutions.

Inflow and outflow boundaries (A–B and D–C)

It is assumed that if the inflow and outflow boundaries are set sufficiently far away from the cylinders, then the velocity components in the direction normal to the symmetry lines are negligible, implying that in the far field all flow must be in the direction parallel to the symmetry lines. This is not strictly true for the outflow section, unless it is considered at a very large distance from the cylinder center. The approach here is to somehow neglect the details of flow further downstream and obtain realistic answers upstream [19]. The boundary conditions for the inflow and outflow sections then become

$$\frac{\partial \bar{\psi}^*}{\partial y^*} = \frac{\partial \bar{\omega}^*}{\partial y^*} = \frac{\partial k^*}{\partial y^*} = \frac{\partial \varepsilon^*}{\partial y^*} = 0. \tag{16}$$

The temperature of the fluid drawn into the flow field is the same as the ambient temperature. However, a generalization along the outflow boundary cannot be made since the temperature distribution is not known *a priori*. It is assumed that the temperature gradient normal to the outflow boundary is zero.

Cylindrical surfaces

The value of the stream function is uniform around any particular cylinder, corresponding with an impermeable wall. Its value is the same as along the adjacent symmetry plane. The thermal boundary condition applied in the present calculations is that of uniform surface temperature around the perimeter of the cylinder. An expression for vorticity at the cylinder wall is obtained by expanding the stream function near the wall as a Taylor series and then using the continuity and the no-slip condition. Thus, the vorticity at the cylinder wall is given by

$$\bar{\omega}^* = \frac{2(\bar{\psi}_w^* - \bar{\psi}^*)}{(\Delta r^*)^2} \tag{17}$$

where $\bar{\psi}_w^*$ is the stream function value at the confining wall and $\bar{\psi}^*$ is the value at a short distance Δr^* into the fluid.

For the turbulent flow predictions, the conditions for k^* and ε^* have to be considered on all boundaries including the cylindrical surfaces. On the cylindrical walls, k^* is set equal to zero. However, the value of ε^* is difficult to assign on the walls because $\varepsilon \sim k^{3/2}/l$ with k and l being both zero at the wall. This dilemma was circumvented by using the wall-function expression for ε^* near the wall [20]. The rate of dissipation of kinetic energy near the walls is fixed by the requirement that

Table 1. Constants used in the turbulence model

C_μ	C_1	C_2	C_3	σ_k	σ_ε	σ_T
0.09	1.44	1.92	1.44	1.0	1.3	1.0

the length scale varies linearly with the distance from the wall. The expression for ε_p^* is

$$\varepsilon_p^* = \frac{C_\mu^{3/4}}{\kappa} \frac{k_p^{*3/2}}{\Delta r_p^*} \tag{18}$$

where the subscript p represents the nearest grid point from the wall, κ is the von Karman constant with a value of 0.42.

Intersections between polar and Cartesian grids

The values of the dependent variables on the "false" polar and Cartesian nodes are obtained by interpolation from the surrounding four Cartesian and polar nodes respectively [5]. These values are then used as the boundary conditions during the next cycle of iteration. The interpolation assumes a linear variation of the dependent variables between the grid nodes, which is a reasonable approximation when the grid intersections are not within the wall boundary layers.

SOLUTION PROCEDURE

Both for the polar and Cartesian grids, the equations (2)–(6) and (9)–(13) are transformed into difference equations by using a finite difference method presented by Gosman *et al.* [11]. Instead of using standard Taylor series expansions, the finite difference equations are obtained by integration over finite cells. The method was developed by its originators for arbitrary orthogonal coordinates, a feature which makes it particularly attractive in the present case where different coordinates are used in different regions. A successive substitution technique is employed to solve the finite difference equations. The finite difference procedure adopts an "upwind" difference treatment of the convective terms and the difference equations are solved by a point iteration method.

The calculations were performed on a Burroughs B7700 digital computer. To obtain converged solutions, about 300 iterations were needed for the laminar cases and about 500 iterations for the turbulent flow predictions. For higher Rayleigh numbers, the solutions of the previous lower Rayleigh number case were used as the initial values in the iterative process (for the same S_L/D and S_T/D ratios).

RESULTS AND DISCUSSION

For a single row of heated cylinders, solutions were obtained both for laminar and turbulent cases. The Nusselt number in this case becomes a function of Rayleigh number as well as the S_L/D ratio. Predictions were obtained for the Rayleigh number (based on cylinder diameter) range of 10^3–10^5 while the ratio S_L/D was varied from 6 to 2. For the case of $S_L/D = 2$, solutions were obtained over an extended Rayleigh number range (10^3–10^9). The predictions for $Ra > 10^7$ were obtained using the k–ε turbulence model discussed earlier.

The inflow and outflow boundaries were considered at a distance $4D$ from the center of the cylinder (for the "single row" case) for the S_L/D ratio of 6. This distance was gradually reduced for decreasing S_L/D ratios to reduce computational time. It is noted here that extending the inflow and outflow boundaries to *very* large distances would invalidate the symmetry boundary conditions used along lines B–C and A–D (as shown in Figs. 1–3). A polar grid of 15 × 31 ($r \times \theta$) near the cylinder and a Cartesian grid of 25 × 49 ($x \times y$) for the remaining area (within the symmetry region shown in Fig. 1) were used for the laminar flow predictions for the "single row" case. For turbulent flow predictions (only for $S_L/D = 2$) a polar grid of 31 × 51 ($r \times \theta$) and a Cartesian grid of 25 × 69 ($x \times y$) were used. The radial node spacing was reduced by a factor of 2 for the nodes close to the cylinder wall as

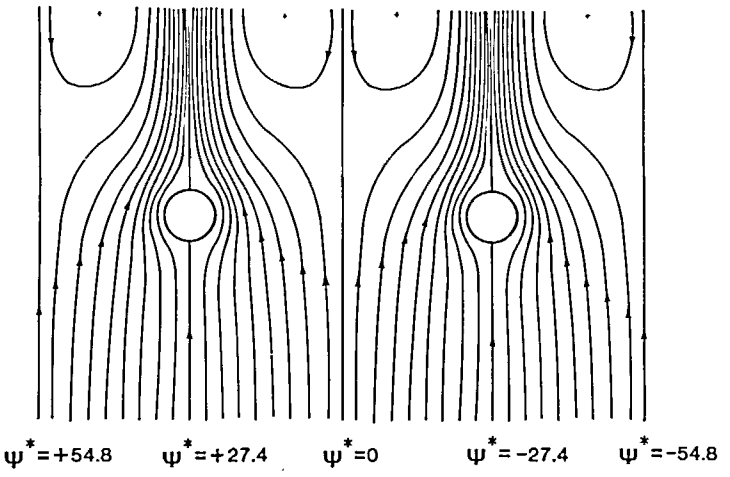

FIG. 4. Streamlines for a single row of cylinders, $Ra = 10^3$, $S_L/D = 6$, $\Delta\psi^* = -3.19$.

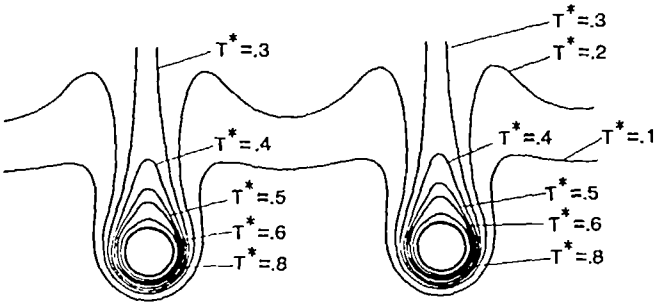

FIG. 5. Isotherms for a single row of cylinders, $Ra = 10^3$, $S_L/D = 6$.

compared to the remaining polar region for both the laminar and the turbulent flow cases. The polar grid extended up to a distance of $2D$ from the center for $S_L/D = 6$.

Figure 4 shows the natural convection flow patterns for a single row of cylinders at $Ra = 10^3$ and $S_L/D = 6$. The results were obtained only for the symmetry region A–B–C–D as shown in Fig. 1. Figure 4 was constructed by joining the solutions of four adjacent symmetry units together. An infinite row is considered and thus end effects were not accounted for. It is observed that as the plume forms at the wake regions of the cylinders, a strong flow reversal is encountered due to the restricted flow region. The isotherms for this flow situation are shown in Fig. 5. If a finite number of cylinders are considered, then much farther downstream the plane of the cylinders, the temperature distribution will no longer resemble plumes arising from individual sources but from a single source [7]. Since a 2-dim., steady-state model is employed, no oscillations in the plume (if they are present) can be predicted. The heat transfer results may not be significantly affected by this.

The heat transfer characteristics for a single row of cylinders at varying S_L/D ratios are presented in Fig. 6. The results are shown over the Rayleigh number range of 10^3–10^5. The results indicate the strong influence of the cylinder spacing on the average Nusselt number. For low Rayleigh numbers the heat transfer is decreased for close spacings of the cylinders. But as the Rayleigh number increases the effect diminishes and can even result in enhanced heat transfer. The optimum spacing for maximum heat transfer was found to be a strong function of the Rayleigh number as is evident from Fig. 6. In all cases, the mean Nusselt number will approach the value for a single cylinder in an unbounded Boussinesq fluid [12] when S_L/D is increased to a large value.

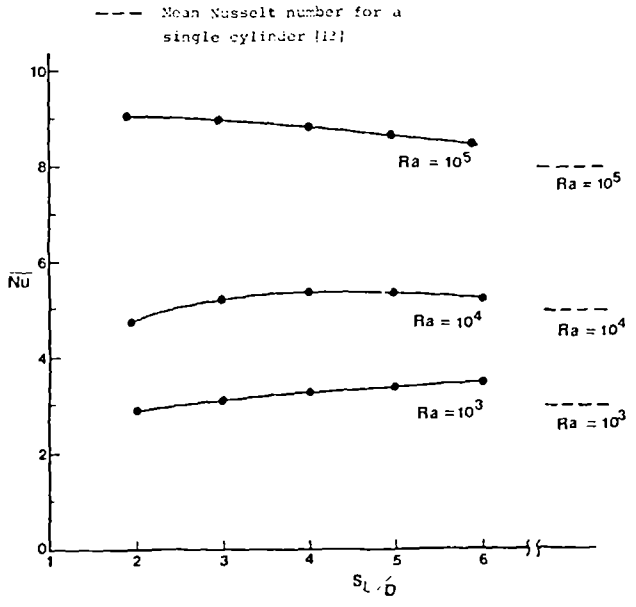

FIG. 6. Mean Nusselt number for a single row of cylinders.

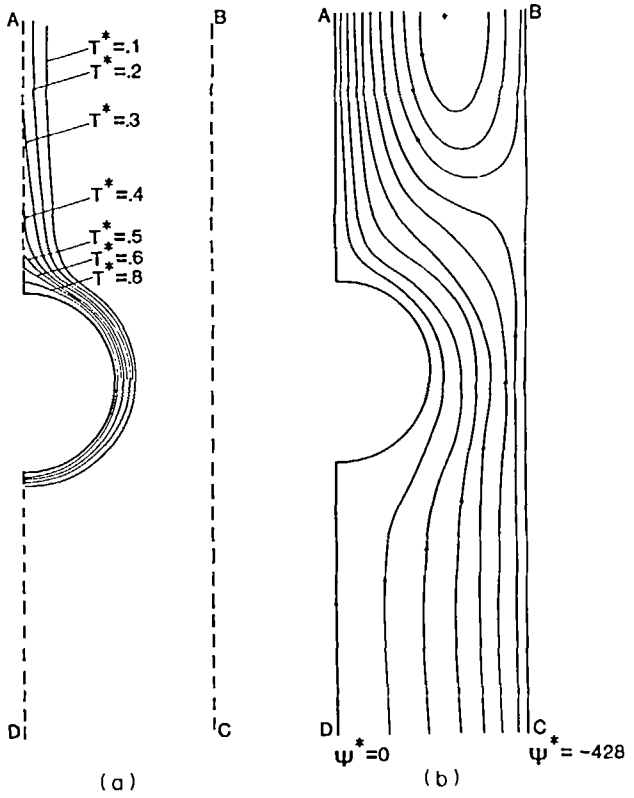

FIG. 7(a). Isotherms for a single row of cylinders, $Ra = 10^6$, $S_l/D = 2$. (b) Streamlines for a single row of cylinders, $Ra = 10^6$, $S_l/D = 2$, $\Delta\psi^* = -60.0$.

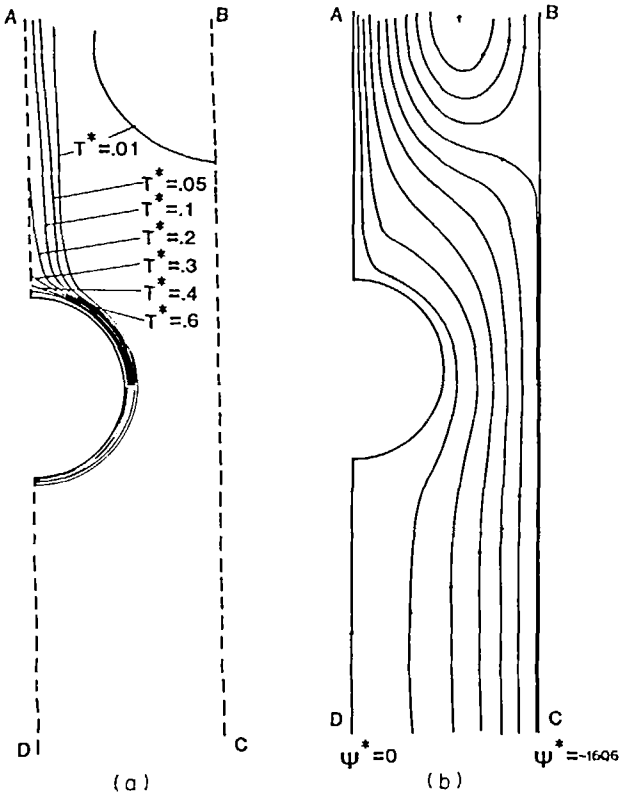

FIG. 8(a). Isotherms for a single row of cylinders (turbulent flow), $Ra = 10^8$, $S_l/D = 2$. (b). Streamlines for single row of cylinders (turbulent flow), $Ra = 10^8$, $S_l/D = 2$, $\Delta\psi^* = -209.6$.

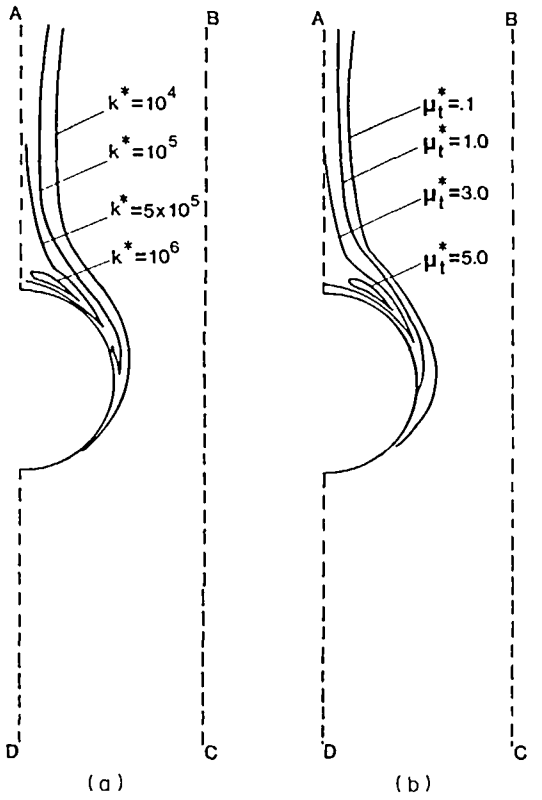

FIG. 9(a). Constant turbulent kinetic energy lines for a single row of cylinders, $Ra = 10^8$, $S_L/D = 2$.
(b). Constant turbulent viscosity lines for a single row of cylinders, $Ra = 10^8$, $S_L/D = 2$.

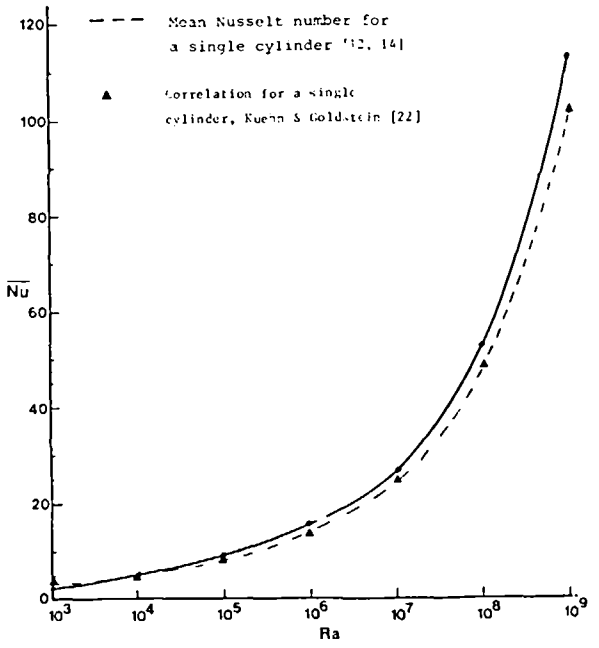

FIG. 10. Mean Nusselt number as a function of Rayleigh number for a single row of cylinders, $S_L/D = 2$.

For the particular case of $S_L/D = 2$, results were obtained beyond the range shown in Fig. 6. Figures 7(a) and 7(b) display the isotherms and flow patterns for a single row of cylinders where $Ra = 10^6$ and $S_L/D = 2$. The results are shown only for the symmetry region as given in Fig. 1. The thermal boundary layer adjacent to the cylinder thins considerably, consistent with previous observations for a single cylinder [12, 21]. The close spacing of the cylinders, however, affects the orientation of the flow patterns. It was observed in the study of the natural convection flow around a single cylinder, that at high Rayleigh numbers, the majority of the flow comes from the sides instead of the bottom [12, 14, 21]. The heat transfer in this case is found to be enhanced by the spacing of the cylinders. More detailed study is needed to verify this conclusion.

Turbulent flow predictions were obtained for single row of cylinders at the S_L/D ratio of 2 and for the Rayleigh number range of 5×10^7 to 10^9. Figures 8(a) and 8(b) show the time-averaged isotherms and streamlines at Rayleigh number of 10^9 for the symmetry region as shown in Fig. 1. The thermal boundary is found to be extremely thin which is in agreement with the results for turbulent natural flow around a single cylinder [14]. The effects of the neighboring cylinders are, however, evident from the streamlines. The constant turbulent kinetic energy lines and the constant turbulent viscosity ($\mu_t^* = \mu_t/\mu$) lines are shown in Figs. 9(a) and 9(b), respectively. The turbulent kinetic energy and the turbulent viscosity are found to be high along the center of the plume and close to the cylinder at the wake region. The heat transfer results for a single row of cylinders at $S_L/D = 2$ are given in Fig. 10 for the Rayleigh number range of 10^3–10^9. The mean Nusselt numbers for a single cylinder placed in an infinite medium are also shown in the same figure from the correlation given by Kuehn and Goldstein [22]. The validity of the present numerical approach has been demonstrated by solving the well documented 'single horizontal cylinder' case, both for the laminar and turbulent flow regimes [12, 14]. The mean Nusselt numbers from the above studies are also shown in Fig. 10 for the purpose of comparison. It is observed that for the single *row* of cylinders, the heat transfer is decreased at low Rayleigh numbers for this S_L/D ratio, but the trend is reversed for higher Rayleigh numbers. This is probably due to the change in flow patterns caused by the spacing of the cylinders. Further work in this area is also needed to validate the observations.

Numerical solutions for the temperature and velocity fields were obtained for the natural convection

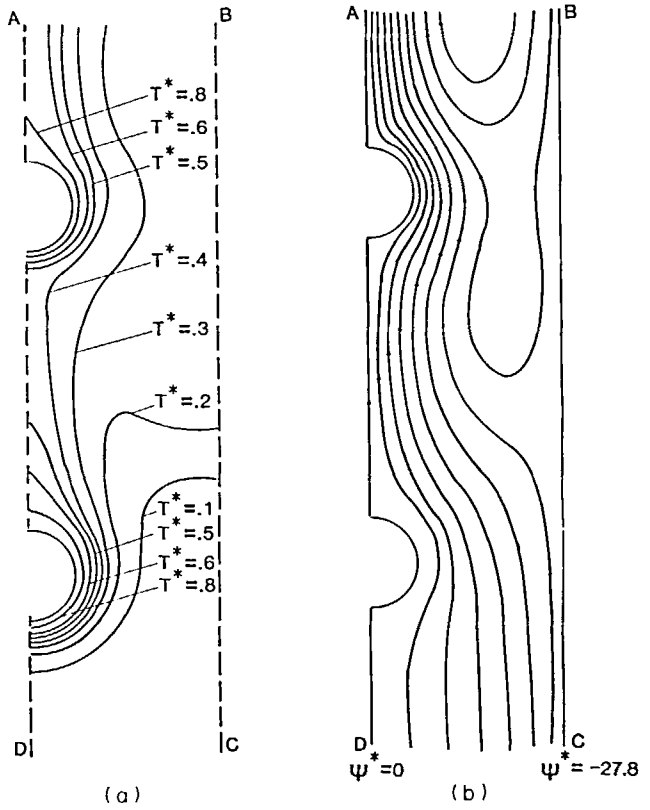

FIG. 11(a). Isotherms for double rows of cylinders (in-line), $Ra = 10^3$, $S_L/D = S_T/D = 4$. (b). Streamlines for double rows of cylinders (in-line), $Ra = 10^3$, $S_L/D = S_T/D = 4$, $\Delta\psi^* = -4.26$.

low around double rows of in-line and staggered cylinders. The symmetry regions as shown in Figs. 2 and 3 were considered. For both the in-line and staggered arrangements, polar grids (15 × 31) were used near the vicinity of the cylinders and the remaining region was filled with a Cartesian grid (25 × 97) system. A limited study was carried out in this case and solutions were obtained only for $S_L/D = S_T/D = 4$ for both the in-line and staggered arrangements. Only laminar flow situations were considered. The inflow and outflow boundaries were considered at a distance of $2D$ from the nearest cylinder. Figures 11(a) and 11(b) show the isotherms and streamlines for natural convection flow in double rows of in-line cylinders at Rayleigh number of 10^3. Both cylinders are maintained at the same constant temperature. The top cylinder is subjected to the warm wake of the bottom cylinder. However, due to the close *horizontal* spacing of the cylinders, a strong flow reversal is observed. The heat transfer results for the in-line arrangement are shown in Fig. 12. Results were obtained for the Rayleigh number range of 10^3–10^5. The mean Nusselt number for the bottom cylinders was about the same as found for the case of single row of cylinders, for the same S_L/D ratio. The mean Nusselt number for the top cylinders was, however, found to be higher than the

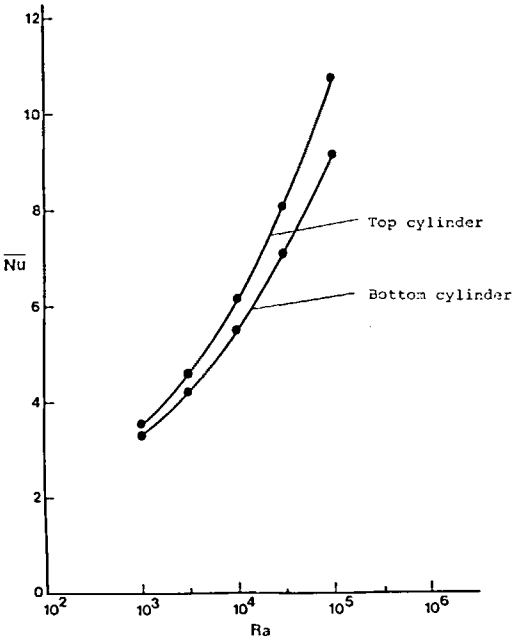

FIG. 12. Mean Nusselt Number for two rows of in-line cylinders, $S_L/D = S_T/D = 4$.

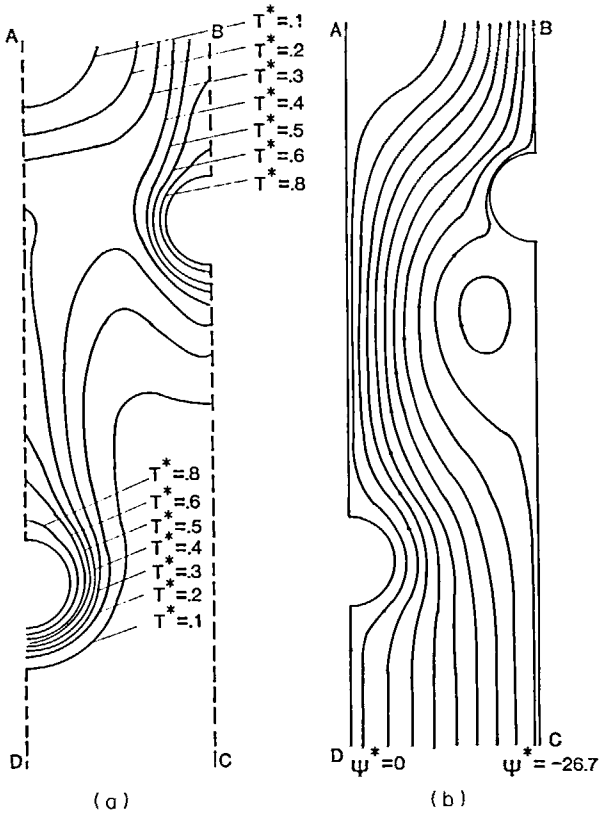

FIG. 13(a). Isotherms for double rows of cylinders (staggered), $Ra = 10^3$, $S_L/D = S_T/D = 4$. (b). Streamlines for double rows of cylinders (staggered), $Ra = 10^3$, $S_L/D = S_T/D = 4$, $\Delta\psi^* = -2.91$.

bottom cylinders. The heat transfer is dependent on S_L/D and S_T/D ratios as well as the Rayleigh number considered. Indeed, the trend may reverse for different cylinder spacings (in the vertical and horizontal direction) as has been observed by Marsters [23], who studied heat transfer properties of a single vertical array of a finite number of heated cylinders in steady state natural convection. Similar observations were also made by Sparrow and Niethammer [24], who studied effects of vertical separation distance on natural convection for a pair of horizontal cylinders.

Figures 13(a) and (b) display the isotherms and streamlines for the staggered arrangement at Rayleigh number of 10^3. Both the top and bottom cylinders are again maintained at the same constant temperature and the results are shown for the symmetry region as depicted in Fig. 3. The S_L/D and S_T/D ratios were kept equal to 4 as was done for the in-line case. The figures reveal interesting details of the complex flow situation. The top cylinder is not completely in the wake of the bottom cylinder. The plume arising from the bottom cylinder is attracted towards the side by the top cylinder and the flow attains a wavy pattern. This, in turn, causes a reduction of the flow reversal encountered in the in-line case. The heat transfer results for the staggered arrangement is given in Fig. 14 where the mean Nusselt number values for the bottom and top cylinders are given for the Rayleigh number range of 10^3–10^5 with $S_L/D = S_T/D = 4$. The mean Nusselt number of the bottom cylinders was found to have increased, compared to the case of a single row of cylinders reported earlier. The Nusselt number for the top cylinders was, however, found to decrease in this case. This is perhaps due to the lesser amount of flow reversal accounted near the outflow regions of the top cylinders. A further detailed study is needed to study the effects of S_L and S_T on the Nusselt numbers and flow fields at various Rayleigh numbers for the in-line and staggered arrangements.

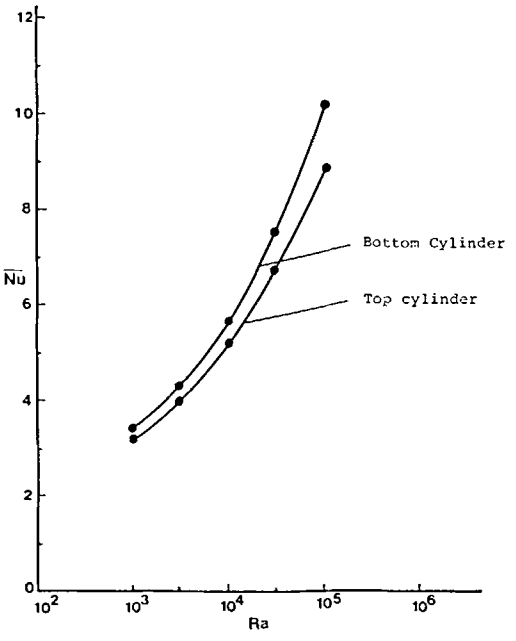

FIG. 14. Mean Nusselt numbers for two rows of staggered cylinders, $S_L/D = S_T/D = 4$.

The results presented in this paper indicate that the complex natural convection flow situations arising out of closely spaced heated cylinders can be analyzed with the numerical technique and the composite grid system used. It was observed that the heat transfer characteristics are strongly dependent on the spacings of the cylinders as well as the Rayleigh number. A detailed numerical study of the problems can be carried out to establish the optimum spacings for maximum heat transfer. Experimental investigations in this area are also needed to further validate the results. Experimental results can, in particular, be used to improve the approximate outflow boundary conditions and the extent of the flow domain to be considered for any future numerical investigations.

REFERENCES

1. A. Zhukauskas, Heat transfer from tubes in cross flow, *Adv. Heat Transfer* **8**, 93–160 (1972).
2. E. D. Grimison, Correlation and utilization of new data on flow resistance and heat transfer for cross flow of gases over tube banks, *Trans. ASME* **59**, 583–594 (1937).
3. O. P. Bergelin, G. A. Brown and S. C. Doberstein, Heat transfer and fluid friction during flow across banks of tubes-IV, *Trans. ASME* **74**, 953–960 (1952).
4. A. Thom and C. J. Apelt, *Field Computation in Engineering and Physics*. Van Nostrand, London (1961).
5. B. E. Launder and T. H. Massey, The numerical prediction of viscous flow and heat transfer in tube banks, *Trans. Am. Soc. Mech. Engrs*, Series C, *J. Heat Transfer* **100**, 565–571 (1978).
6. E. R. G. Eckert and E. Soehngen, Studies on heat transfer in laminar free convection with Zehnder–Mach interferometer, USAF Technical report no. 5745 (1948).
7. J. Lieberman and B. Gebhart, Interactions in natural convection from an array of heated elements, experimental, *Int. J. Heat Mass Transfer* **12**, 1385–1396 (1969).
8. E. Tillman, Natural convection heat transfer from horizontal tube bundles, ASME paper 76-HT-35 (1976).
9. L. Davis and J. Perona, Development of free convection axial flow through a tube bundle, *Int. J. Heat Mass Transfer* **16**, 1425–1438 (1973).
10. R. O. Warrington and G. Crupper, Natural eonvection heat transfer between cylindrical tube bundles and a cubical enclosure, ASME Winter Annual Meeting, New York (1979).
11. A. D. Gosman, W. M. Pun, A. K. Runchal, D. B. Spalding and M. W. Wolfshtein, *Heat and Mass Transfer in Recirculating Flows*. Academic Press, London (1969).
12. B. Farouk and S. İ. Güçeri, Natural convection from a horizontal circular cylinder-laminar regime, *Trans. Am. Soc. Mech. Engrs*, Series C, *J. Heat Transfer* **103**, 522–527 (1981).
13. B. Farouk and S. İ. Güçeri, Laminar and turbulent natural convection in the annulus between horizontal concentric cylinders, *ASME–AIChE Nat. Heat Transfer Conf.* HTD-Vol. 16, 143–150 (1981).

14. B. Farouk and S. İ. Güçeri, Natural convection from a horizontal cylinder-turbulent regime, *J. Heat Transfer* **104**, 228–235 (1982).
15. D. B. Spalding and B. E. Launder, The numerical computation of turbulent flows, *Computer Meth. Appl. Mechanics Engng* **3**, 269–289 (1974).
16. G. D. Raithby and K. G. T. Hollands, A general method of obtaining approximate solutions to laminar and turbulent free convection problems, *Adv. Heat Transfer* **18**, 265–315 (1975).
17. B. Farouk, Laminar and turbulent natural convection heat transfer from horizontal cylinders, Ph.D. thesis, University of Delaware (1981).
18. M. P. Fraikin, J. J. Portier and C. J. Fraikin, Application of a k–ε turbulence model to an enclosed buoyancy driven recirculating flow, ASME paper no. 80-HT-68 (1980).
19. P. J. Roache, *Computational Fluid Dynamics*, pp. 152–161. Hermosa, Alburquerque (1972).
20. D. B. Spalding, Turbulence models (2nd issue), Imperial College of Science and Technology, London, Heat Transfer Section Reports, HTS/76/17, January (1977).
21. T. H. Kuehn and R. J. Goldstein, Numerical solution to the Navier–Stokes equations for laminar natural convection about a horizontal isothermal circular cylinder, *Int. J. Heat Mass Transfer* **23**, 971–979 (1980).
22. T. H. Kuehn and R. J. Goldstein, Correlating equations for natural convection heat transfer between horizontal circular cylinders, *Int. J. Heat Mass Transfer* **19**, 1127–1134 (1976).
23. G. F. Marsters, Arrays of heated horizontal cylinders in natural convection, *Int. J. Heat Mass Transfer* **15**, 921–923 (1972).
24. E. M. Sparrow and J. E. Niethammer, Effect of vertical separation distance and cylinder-to-cylinder temperature imbalance on natural convection for a pair of horizontal cylinders, *J. Heat Transfer* **103**, 683–1981).

CONVECTION NATURELLE AUTOUR DE CYLINDRES HORIZONTAUX DANS DES CHAMPS D'ECOULEMENT INTERACTIFS

Résumé—Le transfert thermique par convection naturelle autour de rangées simples ou doubles de cylindres isothermes et étroitement espacés est étudié numériquement à la fois pour les cas laminaire et turbulent. On considère un nombre suffisammant grand de cylindres dans chaque rangée, de telle sorte qu'une maille symétrique peut être considérée dans cette analyse. Le schéma numérique utilise un réseau cylindrique de noeuds au voisinage du cylindre avec une maille cartésienne couvrant le domaine de l'écoulement. Le modèle k–ε de turbulence est appliqué pour obtenir les résultats sur l'écoulement turbulent. On considère l'effet de l'espacement varié entre cylindres dans la direction horizontale. Les résultats sont utilisables directement dans le chauffage électrique ou solaire, dans la technologie du stockage, dans la sûreté des réacteurs nucléaires parmi d'autres cas.

NATÜRLICHE KONVEKTION AN HORIZONTALEN ZYLINDERN IN WECHSELWIRKUNG MIT STRÖMUNGSFELDERN

Zusammenfassung—Der Wärmeübergang durch natürliche Konvektion von Einzel- und Doppelreihen eng angeordneter isotherm beheizter Zylinder wird numerisch untersucht und zwar für den laminaren und den turbulenten Fall. Dabei wird für jede Reihe eine ausreichend große Anzahl von Zylindern angenommen, wodurch bei der Untersuchung eine symmetrische Einheit betrachtet werden kann. Für das numerische Rechenverfahren wird ein zylindrisches Knoten-Netzwerk in der Nähe des Zylinders und ein kartesisches Netz im restlichen Strömungsgebiet benutzt. Für die Berechnung bei turbulenter Strömung wird das k–ε-Tubulenzmodell verwendet. Auch der Einfluß des Zylinderabstandes in horizontaler Richtung wird betrachtet. Die Ergebnisse sind unter anderem bei elektrischen Anordnungen, bei der Solarheizungs- und Speicher-Technologie, bei der Reaktor-Sicherheit und der Beseitigung radioaktiver Abfälle von direktem Nutzen.

ЕСТЕСТВЕННАЯ КОНВЕКЦИЯ ОТ ГОРИЗОНТАЛЬНЫХ ЦИЛИНДРОВ ВО ВЗАИМОДЕЙСТВУЮЩИХ ПОЛЯХ ТЕЧЕНИЯ

Аннотация—Проведено численное исследование процесса теплопереноса при естественной конвекции от одного и двух рядов плотно расположенных изотермических нагреваемых цилиндров при ламинарном и турбулентном обтекании. В каждом ряду рассматривается достаточно большое число цилиндров для того, чтобы можно было выделить симметричную ячейку для анализа. Численная схема состоит из цилиндрической сетки узловых точек вблизи цилиндра и декартовой сетки в остальной области течения. Для расчета турбулентного течения использовалась турбулентная модель k–ε. Рассмотрено также влияние изменения расстояния между цилиндрами в горизонтальном направлении. Результаты работы могут иметь непосредственное применение в электротехнике, технологии получения и накопления солнечной энергии, для обеспечения безопасности ядерных реакторов и удаления отходов, а также в других областях.